

**Velocity profiles and frictional pressure drop for shear thinning materials in lid driven cavities with fully developed axial flow**

K.-H. Sun<sup>1</sup>, D. L. Pyle<sup>1</sup>, M. J. Baines<sup>2</sup>, N. Hall-Taylor<sup>3</sup>, A. D. Fitt<sup>4\*</sup>

<sup>1</sup> School of Food Biosciences, University of Reading, RG6 6AP, UK

<sup>2</sup> Department of Mathematics, University of Reading, RG6 6AP, UK

<sup>3</sup> Chemtech International Ltd, Reading, RG2 0LP, UK

<sup>4</sup> School of Mathematics, University of Southampton, Southampton SO17 1BJ, UK

**Abstract**

A finite element numerical study has been carried out on the isothermal flow of power law fluids in lid driven cavities with axial throughflow. The effects of the tangential flow Reynolds number ( $Re_U$ ), axial flow Reynolds number ( $Re_W$ ), cavity aspect ratio and shear thinning property of the fluids on tangential and axial velocity distributions and the frictional pressure drop are studied. Where comparison is possible, very good agreements is found between current numerical results and published asymptotic and numerical results. For shear thinning materials in long thin cavities in the tangential flow dominated flow regime, the numerical results show that the frictional pressure drop lies between two extreme conditions, namely the results for duct flow and analytical results from lubrication theory. For shear thinning materials in a lid driven cavity, the interaction between the tangential flow and axial flow is very complex because the flow is dependent on the flow Reynolds numbers and the ratio of the average axial velocity and the lid velocity. For both Newtonian and shear thinning

---

\* Corresponding author: School of Mathematics, University of Southampton, Southampton, SO17 1BJ, UK, Tel: +44 (0)23 8059 5141, Fax: +44 (0)23 8059 5147, Email: adf@maths.soton.ac.uk

fluids the axial velocity peak is shifted and the frictional pressure drop is increased with increasing tangential flow Reynolds number. The results are highly relevant to industrial devices such as screw extruders and scraped surface heat exchangers.

Keywords: Numerical Modelling, Fluid Mechanics, Processing, Non-Newtonian Fluid, Lid Driven Cavity, Axial Flow

### **Nomenclature**

A	cavity aspect ratio $H/L$ (-)
$k_m$	consistency index ( $\text{Pa}\cdot\text{s}^m$ )
$c_1, c_2$	constants in equation (5)
f	friction factor (-)
H	cavity height (m)
$I_2$	second invariant of the rate of deformation tensor (/s)
L	lid side cavity length (m)
m	shear thinning or power law index (-)
p	pressure ( $\text{N}/\text{m}^2$ )
$-p_z$	axial pressure gradient ( $\text{N}/\text{m}^3$ )
$Re_U$	U-Reynolds number $Re_U = \rho UL/\mu_F$
$Re_W$	W-Reynolds number $Re_U = \rho WL/\mu_F$
$S_v, S_w$	convergence criteria (-)
U	lid velocity (m/s)
u	x-component of velocity (m/s)
V	tangential velocity (m/s)
v	y-component of velocity (m/s)
W	average axial velocity (m/s)

$w$	$z$ -component of velocity (m/s)
$x, y, z$	Cartesian coordinates (m)
$\alpha$	velocity ratio or Reynolds number ratio (-)
$\dot{\gamma}$	shear rate (/s)
$\mu$	absolute viscosity (Nm/s <sup>2</sup> )
$\mu_F$	characteristic viscosity (Nm/s <sup>2</sup> )

## 1. Introduction

Fluid flow in lid driven cavities (Shanker and Deshpande (2000)) is an important simplified model of direct relevance to many complex practical flow problems, such as motion in thin film coaters for the production of tape and photographic film (Aidun et al. (1991)), flow in screw extruders for polymer and food processing (Griffith (1962)) and scraped surface heat exchangers for the processing of highly viscous food materials (Harrod (1991)). Most industrial process operations of this sort are three-dimensional low Reynolds number flows that are dominated by the tangential flow. The fact that such processes typically involve non-Newtonian materials means that simulations of the full problem still poses serious challenges. Early studies on cavity flow with Newtonian fluids were reported by Burggraf (1966), Pan and Acrivos (1967) and Nallasamy and Prasad (1977). With improvements in computer power and numerical codes, increasing research activity is taking place on lid driven cavities with non-Newtonian materials, including studies on viscoelastic fluids (Grillet et al. (1999)), Bingham fluids (Mitsoulis and Zisis (2001)) and power law fluids (Marton (1969)).

Using finite element methods, Sun et al. (2003a, 2003b) studied flow and forced convection heat transfer with viscous dissipation in scraped surface heat exchangers with power law shear thinning and heat thinning fluids. A typical scraped surface heat exchanger comprises a central shaft rotating inside a narrow annulus. The outer surface of the annulus is scraped by blades attached to the rotating shaft; the blades are often staged along the axis of the shaft. In steady-state 2D lid driven cavities (Sun et al 2003a), computed finite element results showed that the velocity and temperature distributions are very different for power law and Newtonian fluids. Close to the singularity corners where the cavity lid and sidewalls meet, the local viscosity and viscous dissipation are both reduced with shear thinning fluids. As a result, the local fluid temperature and the heat flux across the lid are both lower for shear thinning fluids than in the corresponding Newtonian fluid. The computations were further extended to study steady state 2D flow in scraped surface heat exchangers with closed and cutaway blades (Sun et al 2003b). These results showed that heat transfer across the outer cylinder was greatly affected by the characteristic viscosity and the variation in the local viscosity due to the shear and heat thinning.

As numerical studies of the full 3D problem with non-Newtonian fluids are still out of reach for most applications it comes as no surprise that existing numerical results are largely limited to simplified steady 2D flows in which the effects of axial flow are neglected. For non-Newtonian fluids the tangential and the axial flows are highly coupled due to their shear dependent rheology. It is important to know the consequences of axial flux and, in particular, how the tangential (cross) flow interacts with the axial flow and how much it affects the power required to pump the fluid. Fitt and Please (2001) provided an asymptotic analysis of the 3D isothermal flow of

power law fluids in lid driven cavities. Lubrication theory was used to study flow in scraped surface heat exchangers with small annular-gap/perimeter ratios. Very useful predictions were made of velocity profiles and the relation between the axial mass flux and frictional pressure drop; also, the optimal energy distribution between rotating and pumping was determined. In an analysis of a related flow problem, Karwe and Jaluria (1990) studied fluid flow and heat transfer in a single screw extruder using finite difference techniques. Creeping flow was assumed in both the axial and the barrel moving directions and the effect of the screw was neglected by assuming a long, shallow channel. The bulk temperature and Nusselt number along the screw helix were obtained for Newtonian and power law fluids with a shear thinning index of 0.5.

The work reported here extends our previous finite element numerical studies to include the effects of axial flow. The flow behaviour in scraped surface heat exchangers provides the context. By assuming isothermal fully developed laminar flow in the axial direction, the interaction between the axial flow and the tangential flow in lid driven cavities is studied. For fully developed laminar flow with Newtonian fluids, the secondary flow, i.e. the tangential flow, decouples from the axial flow. The tangential flow field may be determined first, and then the axial flow field found separately. For non-Newtonian power law fluids the tangential flow and the axial flow fields cannot be determined separately. A simple numerical procedure is used to compute the tangential and axial velocity components and the frictional pressure gradient. The computations aim to extend our basic understanding of power law fluids in lid driven cavities with axial flow. The selection of parameters is relevant to industrial applications in scraped surface heat exchangers.

## 2. The differential equations and numerical procedure

### 2.1. Governing equations

A rectangular coordinate system is used with its origin at the bottom left hand corner of the cavity (Fig. 1a). The x- and y-axes are in the plane of the tangential flow and the z-axis is in the direction of the axial flow. The velocity components are denoted by u, v and w respectively. The lid, of length L, is located at the top of the cavity (y=H) and moves at velocity U in the positive x direction and the y-axis is perpendicular to the lid. The cavity aspect ratio is denoted by  $A=H/L$ . During the computations, to maintain a low Reynolds number at all length scales concerned, the longer wall of the cavity (i.e. the lid length L) is used as the non-dimensional length scale. This should be borne in mind when interpreting results where the dominant velocity gradient is along the y axis. The velocity scales are the lid velocity U for the tangential velocity components u and v, and the average axial velocity W for the axial velocity component w. The scale for pressure is  $\mu_F U/L$ . The characteristic viscosity

$\mu_F$  is taken to be the viscosity given at a shear rate  $\dot{\gamma} = \left( \left( \frac{U}{L} \right)^2 + \left( \frac{W}{L} \right)^2 \right)^{\frac{1}{2}}$ . Again, for

cases where  $L > H$  and the gradients in the y- direction dominate those in the x- direction this scaling may have to be altered, though since our results are solely numerical this should not matter in the present study.

We consider isothermal, laminar, steady flows of an incompressible viscous fluid with fully developed axial flow in an infinitely long cavity. It is reasonable to assume that all the velocity components are functions of x and y only, and, from the w momentum

equation, the axial pressure gradient is therefore also independent of  $z$ . At any cross section in the  $x$ - $y$  plane the non-dimensional governing equations are therefore:

The continuity equation

$$\frac{\partial u^*}{\partial x^*} + \frac{\partial v^*}{\partial y^*} = 0 \quad (1)$$

u-momentum equation

$$Re_U \left( u^* \frac{\partial u^*}{\partial x^*} + v^* \frac{\partial u^*}{\partial y^*} \right) = -\frac{\partial p^*}{\partial x^*} + \frac{\partial}{\partial x^*} \left( \frac{\mu}{\mu_F} \frac{\partial u^*}{\partial x^*} \right) + \frac{\partial}{\partial y^*} \left( \frac{\mu}{\mu_F} \frac{\partial u^*}{\partial y^*} \right) \quad (2)$$

v-momentum equation

$$Re_U \left( u^* \frac{\partial v^*}{\partial x^*} + v^* \frac{\partial v^*}{\partial y^*} \right) = -\frac{\partial p^*}{\partial y^*} + \frac{\partial}{\partial x^*} \left( \frac{\mu}{\mu_F} \frac{\partial v^*}{\partial x^*} \right) + \frac{\partial}{\partial y^*} \left( \frac{\mu}{\mu_F} \frac{\partial v^*}{\partial y^*} \right) \quad (3)$$

w-momentum equation

$$Re_U \left( u^* \frac{\partial w^*}{\partial x^*} + v^* \frac{\partial w^*}{\partial y^*} \right) = f Re_W + \frac{\partial}{\partial x^*} \left( \frac{\mu}{\mu_F} \frac{\partial w^*}{\partial x^*} \right) + \frac{\partial}{\partial y^*} \left( \frac{\mu}{\mu_F} \frac{\partial w^*}{\partial y^*} \right) \quad (4)$$

where  $*$  denotes that the variables are in their non-dimensional form,  $Re_U = \frac{\rho UL}{\mu_F}$  is

the tangential Reynolds number,  $Re_W = \frac{\rho WL}{\mu_F}$  is the axial flow Reynolds number,

(equivalent to a non-dimensional axial volume flux), and  $f = \frac{-p_z L}{\rho W^2}$  is the non-

dimensional axial pressure gradient or friction factor. The frictional pressure gradient

is defined as

$$f \cdot Re_W = \frac{-p_z L}{\rho W^2} \cdot \frac{\rho WL}{\mu_F} = \frac{-p_z L^2}{\mu_F W}.$$

The velocity ratio or Reynolds number ratio is  $\alpha = \frac{W}{U} = \frac{Re_w}{Re_U}$ . As the tangential flow is dominant in many industrial applications such as SSHEs and screw extruders, values of the velocity ratio less than one were used in the computations.

The boundary conditions in the plane of the tangential flow are

At the lid  $u^* = 1, v^* = w^* = 0$

At the walls  $u^* = v^* = w^* = 0$ .

A generalized shear thinning power law viscosity  $\mu = k_m I_2^{(m-1)/2}$  is used (Bird et al 1987). Here  $k_m$  denotes the consistency index (Pa-s<sup>m</sup>), which varies with the material.  $I_2$  is the second invariant of the shear rate tensor. Non-dimensionalized by the

characteristic viscosity  $\mu_F = k_m \left( \left( \frac{U}{L} \right)^2 + \left( \frac{W}{L} \right)^2 \right)^{(m-1)/2}$  the final form of the viscosity is

$$\frac{\mu}{\mu_F} = \left( \frac{I_2^*}{(1 + \alpha^2)} + c_1 \right)^{(m-1)/2} + c_2 \quad (5)$$

where  $I_2^* = \left( 2 \left( \frac{\partial u^*}{\partial x^*} \right)^2 + 2 \left( \frac{\partial v^*}{\partial y^*} \right)^2 + \left( \frac{\partial u^*}{\partial y^*} + \frac{\partial v^*}{\partial x^*} \right)^2 + \alpha^2 \left( \frac{\partial w^*}{\partial x^*} \right)^2 + \alpha^2 \left( \frac{\partial w^*}{\partial y^*} \right)^2 \right)$ .

The constants  $c_1$  and  $c_2$  are included to ensure that the viscosity has a nonzero finite value throughout the computational domain. Values of  $c_1=0.000001$  and  $c_2=0.0001$  were selected; numerical experiments show that this modification has an insignificant effect on the bulk viscosity whilst giving physically reasonable viscosity values. The

shear-thinning index  $m$  varies with the material:  $m=1$  corresponds to a Newtonian fluid, while for shear thinning non-Newtonian fluids  $m<1$  (a typical value of  $m$  for food materials such as fruit jam, peanut butter etc. is 0.33). Unless otherwise specified, the results presented below are non-dimensional values with the \* omitted for brevity.

## 2.2. Numerical formulation and solution procedure

The non-dimensional partial differential equations are solved numerically with the commercial finite element partial differential equation solver Fastflo<sup>TM</sup> (2000) using the Galerkin form of the weighted residual finite element formulation. Fastflo<sup>TM</sup> is not a “black box” CFD package. The selected numerical methods have to be implemented through user programming. A detailed discussion of the numerical formulation may be found in Sun et al. (2003a). To solve for the tangential flow field, the augmented Lagrangian method (Sun et al (2003a), Fastflo (2000)) is used. The basic computer code implemented here is the same as that used for the previous case (Sun et al 2003a) except that the viscosity is now also a function of axial shear rate. The Newton-Raphson method is used to compute the axial velocity  $w$  and frictional pressure gradient  $f_{Re_w}$ . The solution algorithm may be summarised as follows:

1. Set the flow parameters: lid velocity, average axial velocity, power law index and number of iterations for Loop 1 and Loop2 etc.
2. Assume an initial axial and tangential velocity distribution
3. (Loop 1) Compute the tangential velocity components  $u(x, y)$ ,  $v(x, y)$  and the pressure  $p(x, y)$  in a 2D cavity
  - a. Calculate the shear dependent viscosity

- b. Solve the continuity equation and  $u$ ,  $v$  momentum equations along with the given velocity boundary conditions, using the augmented Lagrangian method, to obtain the velocity components ( $u$  and  $v$ ) and the pressure  $p$
4. (Loop 2): Calculate the axial velocity and frictional pressure gradient using the Newton-Raphson method
  - a. Assume an initial frictional pressure gradient distribution
  - b. Update the viscosity from the known velocity components
  - c. Solve the  $w$ -momentum equation along with the given boundary conditions
  - d. Calculate the frictional pressure gradient distribution from the updated  $w$ -velocity
  - e. Update the frictional pressure gradient distribution by multiplying by a factor i.e. the ratio between the initial value of average axial velocity and the calculated value
  - f. Repeat steps (b), (c), (d) and (e) to obtain the axial velocity and frictional pressure gradient
5. (Loop 3): Repeat steps (3) and (4) until all the  $u$ ,  $v$  and  $w$  velocities have converged
6. Calculate the streamlines (see section 3.3) for tangential flow from the  $u$  and  $v$  velocity components and the average frictional pressure gradient.

Numerical experiments show that the results and the convergence are not very sensitive to the initial distributions of the axial and tangential velocity. The initial distributions of the axial and tangential velocity are assumed to be uniform in the bulk

with values of 1 and 0, respectively. The initial distribution of the frictional pressure gradient in the bulk is also assumed to be uniform with a value of  $0.18 \cdot m$ , where  $m$  is the power law index.

As mentioned earlier, for power law fluids the  $u$ ,  $v$  and  $w$  momentum equations are coupled so that it is unwise to devote too much time to achieve convergence of the  $u$  and  $v$  velocity components in Loop 1 when these are based on a rough value of the  $w$  velocity component. So Loop 1 and 2 are set to a limited number of iterations to ensure that the  $u$ ,  $v$  and  $w$  velocities converge gradually together. Loop 3 stops if the relative difference between successive solutions for  $u$ ,  $v$  and  $w$  satisfies the convergence criteria.

$$\sum |V_n - V_{n-1}| / \sum |V_n| < S_V \quad (6)$$

$$\sum |w_n - w_{n-1}| / \sum |w_n| < S_w \quad (7)$$

where  $V_n$  and  $V_{n-1}$  are the tangential velocities (from  $u$  and  $v$  components) given by consecutive iterations and  $w_n$  and  $w_{n-1}$  are values of axial velocity in consecutive iterations. Numerical experiments show that for decreasing  $m$  the values of  $S_V$  and  $S_w$  tend to increase (the minimum  $m$  attempted with this computation is 0.2). Their values are also dependent on the cavity aspect ratio. Here different values are set for the convergence criteria with different power law indices:

For large power law indices ( $m \geq 0.4$ )  $S_V = 0.000001, S_w = 0.000001$

and for small power law indices ( $m < 0.4$ )  $S_V = 0.0001, S_w = 0.00001$

The sensitivity of the final value of the frictional pressure gradient to the mesh size and the convergence criteria was carefully checked. The numerical accuracy was

assessed by comparing the calculations with available analytical solutions and, in their absence, with values determined by using Richardson extrapolation (Roache 1997). Richardson extrapolation is applied to the values of the frictional pressure gradient for a group of four selected grids to obtain a final value of even higher accuracy than that for the finest grid. It is found that a mesh concentrated at the cavity surfaces and the singularity corners as in Sun et al. (2003a) provides satisfactory results. The final mesh contains 3470 6-noded triangular elements and is concentrated at all surfaces and also at the singularity corners (Fig. 1b). This mesh provides sufficient resolution at the centre and in the velocity boundary layer for the Reynolds numbers ( $<100$ ) covered in this computation. Convergence was normally achieved within 15 iterations for all of the power law indices studied.

### **3. Results and discussion**

#### *3.1. Effects of axial flow and aspect ratio on pressure gradient in axial direction at $Re_U=1$*

For comparison, the current numerical results are plotted against published results for flow in an infinitely long cavity by Fitt and Please (2001) and for duct flow by Hartnett and Kostic (1989). These previous results are briefly discussed in the appendix. From Fig. 2 to Fig. 5, unless otherwise specified, the solid lines represent the analytical results from lubrication theory by Fitt and Please (2001) (equation (A2)), the dotted lines are the duct flow results by Hartnett and Kostic (1989) (equation (A4)) and symbols denote the numerical results.

For a cavity aspect ratio  $A=0.1$ , the friction factor  $f$  is plotted in Fig. 2 as a function of  $Re_w$  for various values of  $m$ . It shows that for a shear thinning fluid, the friction factor (the non-dimensional pressure gradient in the axial direction) is lower and less

sensitive to  $Re_w$  (the non-dimensional axial volume flux) than for a Newtonian fluid. Very good agreement is found between current numerical results (symbols) and the results from Fitt and Please (2001) (solid lines). The results are also qualitatively consistent with isothermal results for flow in screw extruders found by Griffith (1962). Figs. 3 show the effect of axial flow on the frictional pressure gradient  $f_{Re_w}$  as a function of  $m$  for  $A=0.05, 0.1$  and  $0.25$ , respectively (Fig. 3b shows the same set of data as in Fig. 2). It is seen that for Newtonian fluids, the numerical results are very close to the duct flow results for all the velocity ratios and aspect ratios studied. For shear thinning fluids, the computed frictional pressure gradient is always higher in the lid driven cavity than in duct flow. At low Reynolds numbers, with Newtonian fluids the tangential flow has little effect on the frictional pressure gradient while for shear thinning fluids i.e.  $m < 1$  the frictional pressure gradient increases with the tangential flow. The magnitude of the increase depends on the velocity ratio. For  $Re_U=1$  at a small aspect ratio ( $A=0.05$ ) and small velocity ratio ( $\alpha < 0.2$ ), very good agreement is found between the numerical results and the analytical results from lubrication theory. For strongly shear thinning fluids at high velocity ratio ( $\alpha > 0.2$ ), there is an increased difference between the numerical results and the lubrication results as seen from Fig 3, indicating that the additional shear thinning effect of the axial velocity component on the local viscosity cannot be neglected under these conditions. These figures also show that for Newtonian fluids at high aspect ratio ( $A > 0.1$ ) the effect of the sidewalls cannot be neglected. Interestingly, there is a set of intersection points at a certain value of power law index  $m$  where the results from lubrication theory by Fitt and Please (2001) and the numerical calculations are the same. This is caused by the combined effects from the axial flow on local viscosity and from the cavity sidewalls: increasing the aspect ratio increases the effect of side walls so that the dominant effect

of the cavity lid decreases; thus the actual frictional pressure gradient is higher than that predicted by the lubrication theory results. The viscosity decreases with increased shear thinning (i.e. as  $m$  reduces) and decreases further when axial flow is taken into account; thus the actual frictional pressure gradient is lower than the lubrication results at smaller  $m$ .

### *3.2. Effects of Reynolds numbers, velocity ratio and shear thinning index on frictional pressure drop and velocity profile for $A=0.25$*

For  $Re_w=1$ , the effects of tangential flow Reynolds number  $Re_U$  on the frictional pressure gradient are examined in Fig. 4. The lubrication theory results by Fitt and Please (2001) and duct flow results by Hartnett and Kostic (1989) are also plotted. The results show that the frictional pressure gradient increases as the tangential flow Reynolds number increases. The largest differences occur for more strongly shear thinning fluids (smaller  $m$ ). At relatively low tangential flow Reynolds numbers ( $Re_U < 5$ ) for shear thinning fluids with  $m < 0.6$  the numerical results lie between the results for lubrication theory and those for duct flow. For  $m=0.33$  the effects of the two Reynolds numbers on the friction factor are shown in Fig. 5 which shows that the frictional pressure gradient increases with increasing tangential flow Reynolds number. This is discussed further in section 3.3 below.

The  $u$  and  $w$  velocity component profiles on the cavity centreline ( $x=0.5$ ) for  $Re_U=10$  and  $\alpha=0.2$  are shown in Fig. 6. It is seen that the  $u$  velocity profiles are flattened for shear thinning fluids. For more strongly shear thinning fluids (smaller  $m$ ) the values of the  $u$  and  $w$  velocity components are higher close to the lid ( $y=0.25$ ) because the apparent viscosity is lower here. For  $m=0.33$ , the effect of velocity ratio on the cavity

centreline  $u$  and  $w$  velocity component profiles is shown in Fig. 7. For tangential flow dominated conditions (small velocity ratio), the asymmetry in the  $w$  profile is more obvious as shown in Fig. 7b. With increasing velocity ratios, the axial flow becomes dominant; the  $u$ -velocity profiles change very little while the location of the maximum  $w$  velocity component moves towards the centre of the cavity, and the axial velocity profile tends to the axisymmetric form found in duct flow.

### *3.3. Effects of tangential flow Reynolds number and velocity ratio on the tangential flow streamlines, axial velocity and viscosity distributions ( $A=0.5$ )*

In this section, contour plots are given for an aspect ratio of 0.5 so as to give more detailed information on the flow field and its behaviour close to the corners in particular. It is worth mentioning that in three dimensions flow streamlines in a cross section are disconnected points: the streamlines displayed in this text are quasi-streamlines for tangential flow which are computed from the corresponding tangential velocity components. The difference in magnitude between successive lines is the same in each plot and higher contour values are always represented by lighter lines. For streamlines and axial velocity, the contour values are zero on the surfaces and the value of consecutive lines increases (for axial velocity) or decreases (for streamlines) monotonically, therefore only the inner-line contour values are given on the figures. For the dimensionless pressure and dimensionless viscosity distributions (normalized by the characteristic viscosity) the detailed contour values are listed on the plots.

For Newtonian fluids with fully developed flow in the axial direction, the tangential flow is independent of the axial flow, although the reverse is not true. Changes with tangential Reynolds number in the tangential flow streamlines, pressure distributions

in the plane of tangential flow and the axial velocity distributions are displayed in Fig. 8 for  $m=1$  with  $Re_U=1$  and 100, respectively. At low tangential Reynolds number the tangential secondary flow, pressure and axial velocity component are close to symmetrical as shown in Figs. 8a, 8c and 8e. On increasing the tangential Reynolds number, the tangential flow circulation zone moves towards the downstream singularity corner (Fig. 8b) while the axial velocity peak is shifted in the opposite direction away from the downstream singularity corner (Fig. 8f). The pressure distribution is shifted owing to the strong tangential circulation (Fig. 8d).

For shear thinning fluids, the tangential and axial flows interact with each other and the final flow picture depends on the tangential Reynolds number, the axial Reynolds number and the velocity ratio. For  $m=0.33$  and  $Re_U=1$  at velocity ratios of 0.2 and 1.0, the tangential flow streamlines, pressure distribution, axial velocity distribution and normalized viscosity are shown in Fig. 9. At a velocity ratio of 0.2, the centres of both the tangential flow streamlines (Fig. 9a) and the axial velocity (Fig. 9e) are closer to the lid than for the Newtonian case (Figs. 8a and 8e). This is consistent with the  $u$  and  $w$  velocity profiles shown in Fig. 6. When the velocity ratio is increased, the centres of the tangential flow streamlines (Fig. 9b) and the axial velocity (Fig. 9f) shift towards the cavity geometry centre. This is consistent with the velocity profiles shown in Fig. 7. As for strongly shear thinning fluids, the axial velocity profile is highly flattened, the principal contribution of the axial velocity to shear thinning of the viscosity being close to all the surfaces. Thus, with increasing velocity ratio, the apparent viscosity is further reduced, especially close to the surfaces (Fig 9h).

For  $m=0.33$  and  $Re_U=100$  at velocity ratios of 0.01 and 0.2, the tangential flow streamlines, pressure, axial velocity and normalized viscosity are shown in Fig. 10. For shear thinning fluids (Figs. 10a and 10b), the centre of the tangential flow circulation shifts further towards the downstream singularity corner than for Newtonian fluids (Fig. 8b). This is also reflected in the pressure distributions in Figs. 10c and 10d. Figs. 10e and 10f show that the axial velocity peak is shifted with velocity ratio. Numerical experiments indicate that the location of the axial velocity peak also depends upon the Reynolds numbers and the apparent viscosity distribution. At low velocity ratios, the axial velocity peak is close to the downstream singularity corner. With increasing velocity ratio, the axial velocity peak shifts towards the upstream singularity corner. Figs. 10g and 10h show that the location of the viscosity peak also changes with velocity ratio. At high tangential Reynolds numbers and low velocity ratios ( $\alpha < 0.01$ ), the shear thinning is controlled by the velocity gradients in the tangential secondary flow. The strong flow near the downstream singularity corner causes a reduction in apparent viscosity in that region and the apparent viscosity centre peak (distinguished from the apparent viscosity peaks at the stagnation corners) is close to the upstream singularity corner (Figs 10g and 10h).

From the above discussion we can see that in lid driven cavities with axial flow the flow exhibits complex behaviour. The axial flow is distorted by the tangential flow and the effect intensifies with increasing tangential flow Reynolds number. As a result, the frictional pressure drop is increased with increasing tangential flow Reynolds number. The increase is profound for strongly shear thinning fluids, the complex interaction between the tangential and axial flow leading to complex distributions in local viscosity and a substantial increase in the frictional pressure

gradient at high tangential Reynolds number, as shown in Figs. 4 and 5. During these computations, the flow is assumed to be both steady and stable. Further investigations relating to flow stability at high tangential Reynolds numbers are clearly worthwhile, but are beyond the scope of this text.

#### **4. Conclusions**

The finite element method has been used successfully to study fully developed isothermal flow of power law fluids in lid driven cavities with axial throughflow. A simple numerical procedure is used to calculate the tangential and axial velocities and the frictional pressure drop in a lid driven cavity. The effects of tangential and axial Reynolds numbers, the velocity ratio, the cavity aspect ratio and the shear thinning property of the fluids on the flow field and frictional pressure drop are studied. Where comparison is possible, very good agreement is generally found between the numerical results and published analytical, asymptotic and numerical results. It is found that with more strongly shear thinning fluids ( $m < 0.6$ ), for tangential flow dominated ( $\alpha < 0.2$ ) low Reynolds number flow, the frictional pressure drop in thin long cavities lies between the analytical results based on lubrication theory (where the axial flow was negligible) by Fitt and Please (2001) and duct flow results by Hartnett and Kostic (1989).

In a lid driven cavity the  $u$  and  $w$  velocity profiles are both flattened with power law fluids in comparison with the profiles obtained for Newtonian fluids. The tangential flow interacts intensely with the axial flow. At high tangential Reynolds number the increasing distortion in the axial velocity leads to an increase in frictional pressure drop and this happens for both Newtonian and non-Newtonian fluids. For power law

fluids, the interaction between the tangential and axial flow leads to complex distributions of axial velocities and apparent viscosity, and a substantial increase in the frictional pressure gradient.

In this research, a range of parameters has been studied with the intention of extending our basic understanding of power law fluid flows in lid driven cavities with axial flow. The results can be used to interpret the behaviour of screw extruders or scraped surface heat exchangers.

#### **Acknowledgements:**

This research is supported by The University of Reading and Chemtech International Ltd. We are grateful to Professor C. P. Please from the Faculty of Mathematical Studies, University of Southampton for his continued support throughout this research.

#### **Appendix. Frictional pressure gradient for two extreme conditions in a rectangular geometry**

1. Creeping flow in an infinitely long cavity with power law fluids (*valid whenever  $ReUA^2 \ll 1$ ,  $A \ll 1$  and  $\alpha \ll 1$* )

Fitt and Please (2001) provided analytical results for the motion of power law fluids in thin, long cavities. Assuming a small reduced Reynolds number flow in an infinitely long cavity, the inertia terms in the flow equations and the cavity end effects can be neglected. The contribution of axial flow to the shear thinning viscosity is also neglected by assuming that tangential flow is dominant. Analytical results may then

be obtained from lubrication theory. The analytical results give the average axial velocity as

$$W = \frac{-p_z H^{1+m} U^{1-m}}{c_m} f(m) \quad (\text{A1})$$

where  $m$  is the shear-thinning index,  $H$  is the gap width or height of the cavity,  $U$  is the lid velocity and  $-p_z$  is the axial pressure gradient.  $f(m)$  is a (known) function of  $m$  which also depends on the (known) location of the minimum  $u$  velocity. Values of the function  $f(m)$  for selected values of  $m$  are listed in Table 1.

The non-dimensional frictional pressure gradient can be obtained from equation (A1) as

$$fRe_w = -\frac{L^2 p_z}{\mu_F W} = \left(\frac{L}{H}\right)^{m+1} \frac{1}{f(m)} = g_l(m, A) \quad (\text{A2})$$

where  $g_l(m, A)$  is a (known) function of  $m$  and the cavity aspect ratio  $A$ .

For Newtonian fluids, the average axial velocity is  $W = \frac{-p_z H^2}{12\mu_F}$  and the non-

dimensional frictional pressure gradient is  $fRe_w = -\frac{L^2 p_z}{\mu_F W} = 12\left(\frac{L}{H}\right)^2$ .

## 2. Flow in a rectangular duct with power law fluids (*For $Re_U \ll 1$ and $\alpha \gg 1$* )

For fully developed laminar flow of power law fluids in a rectangular duct, the frictional pressure gradient was given by Hartnett and Kostic (1989) as

$$f_d Re_d = 2^{3m+1} \left(a + \frac{b}{m}\right)^m \quad (\text{A3})$$

where the friction factor in a duct is defined as  $f_d = \frac{\tau_w}{\frac{1}{2}\rho W^2} = \frac{-p_z D_H}{2\rho W^2}$ , the Reynolds

number for duct flow is  $Re_d = \frac{\rho W D_H}{\mu_F}$  and  $D_H = \frac{4A}{P} = \frac{2LH}{L+H}$  is the hydraulic

diameter of the duct: a and b are constants that depend on the duct aspect ratio.

Equation (A3) can be expressed as

$$f Re_w = 2 \left( \frac{L}{D_H} \right)^2 f_d Re_d = g_d(m, A) \quad (A4)$$

where  $g_d(m, A)$  is a function of the shear thinning index  $m$  and cavity aspect ratio  $A$ .

It is seen that in both cases, the non-dimensional frictional pressure gradient is a function only of  $m$  and  $A$  as expressed in equations A2 and A4. The relation between  $f Re_w$  and  $m$  is plotted in Fig. A1. It is seen that the value of the non-dimensional frictional pressure gradient  $f Re_w$  increases with increasing power law index  $m$  or with decreasing aspect ratio  $A$ . Interestingly, there is always an intersection point at each aspect ratio where the two values are the same.

## References

- Aidun, C.K., Triantafillopoulos, N.G. and Benson, J.D. (1991). Global stability of a lid-driven cavity with through flow: flow visualization studies. *Phys. Fluids A*, 3:2081-2091
- Bird, R.B., Armstrong, R.C. and Hassager, O. (1987). *Dynamics of polymeric liquids*, Vol 1, in Fluid Mechanics, 2nd edn. John Wiley, New York
- Burggraf, O.R. (1966). Analytical and numerical studies of the structure of steady separated flows. *J. Fluid Mech.*, 24:113-151

- Fastflo Tutorial Guide V3*, (2000). Oxford, Numerical Algorithms Group
- Fitt, A.D. and Please, C.P. (2001). Asymptotic analysis of the flow of shear-thinning food stuffs in annular scraped heat exchangers. *J. Eng. Math.*, 39:345-366
- Griffith, R.M. (1962). Fully developed flow in screw extruders. *IEC Fund.*, 1:180-187
- Grillet, A.M., Yang, B., Khomani, B. and Shaqfeh, E.S.G. (1999). Modelling of viscoelastic lid driven cavity flow using finite element simulations. *J. Non-Newtonian Fluid Mech.*, 88:99-131
- Harrod, M. (1991). Methods to distinguish between laminar and vortical flow in scraped surface heat exchangers. *J Food Proc. Eng.*, 1990, 13(1):39-59
- Hartnett, J.P. and Kostic, M. (1989). Heat transfer to Newtonian and non-Newtonian fluids in rectangular ducts. *Adv. in Heat Transfer*, 19:247-356
- Karwe, M.V. and Jaluria, Y. (1990). Numerical simulation of fluid flow and heat transfer in a single screw extruder for non-Newtonian fluids. *Numerical heat transfer A* (17):167-190
- Martin, B. (1969). Numerical studies of steady state extrusion process. *PhD thesis* Cambridge University
- Mitsoulis, E. and Zisis, T. (2001). Flow of Bingham plastics in a lid driven cavity. *J. Non-Newtonian Fluid Mech.*, 101:173-180
- Nallasamy, M. and Prasad, K.K. (1977). On cavity flow at high Reynolds numbers. *J. Fluid Mech.*, 79:391-414
- Pan, F. and Acrivos, A. (1967). Steady flows in rectangular cavities. *J. Fluid Mech.*, 28:643-655
- Roache, P.J. (1997). Quantification of uncertainty in computational fluid mechanics. *Ann. Rev. Fluid Mech.*, 29:123-160

Shankar, P.N. and Deshpande, M.D. (2000). Fluid mechanics in the driven cavity.  
*Ann. Rev. Fluid Mech.*, 32:93-136

Sun, K.-H., Pyle, D.L., Fitt, A.D., Please, C.P., Hall-Taylor, N. and Baines, M.  
(2003a), Numerical modelling of non-Newtonian heat transfer with viscous  
dissipation in lid driven cavities. (In preparation)

Sun, K.-H., Pyle, D.L., Fitt, A.D., Please, C.P., Baines, M. and Hall-Taylor, N.  
(2003b). Numerical Study of 2D Heat Transfer in a Scraped Surface Heat Exchanger.  
*Int. J. Computers and Fluids*. (to be published)

## Figure Legend

Fig. 1. (a) schematic view of the cavity, (b) mesh at aspect ratio  $A=0.5$  with 3470 elements.

Fig. 2. Friction factor  $f$  as a function of  $Re_W$  for various value of power law index  $m$   $A=0.1$  and  $Re_U=1$ . Solid lines: lubrication theory; Symbols: computed values.

Fig. 3. Frictional pressure gradient at  $Re_U=1$ : (a)  $A=0.05$  and (b)  $A=0.1$  shows the effect of  $Re_W$  and  $m$ , (c)  $A=0.25$  the effect of velocity ratio. Solid lines: lubrication theory by Fitt and Please (2001); Dotted lines: duct flow results by Hartnett and Kostic (1989); Symbols: computed values.

Fig. 4. Effect of tangential flow Reynolds number on  $fRe_W$  for  $A=0.25$  and  $Re_W=1$ . Solid lines: lubrication theory; Dotted lines: duct flow; Symbols: computed values.

Fig. 5. Effect of tangential flow Reynolds number on  $f$  for  $A=0.25$ ,  $m=0.33$ .

Solid lines: lubrication theory; Dotted lines: duct flow; Symbols: computed values.

Fig. 6. Effect of shear thinning index  $m$  on the velocity profiles at the cavity centreline  $x=0.5$  for  $A=0.25$ ,  $Re_U=10$  and  $U/W=0.2$ . (a)  $u$  velocity component (b)  $w$  velocity component.

Fig. 7. Effect of velocity ratio on the velocity profiles at the cavity centreline  $x=0.5$  for  $A=0.25$ ,  $Re_U=10$ ,  $m=0.33$  and  $W/U=0.2$ . (a)  $u$  velocity component (b)  $w$  velocity component.

Fig 8. Effect of tangential flow Reynolds number on the tangential flow streamlines (top) pressure distribution (middle) and axial velocity profile (bottom) for  $A=0.5$  and  $Re_W=1$  with Newtonian fluid  $m=1$ . (a), (c), (e)  $Re_U=1$ , (b), (d), (f)  $Re_U=100$ . For streamlines and axial velocity the contour values at the surface are zero, only the maximum/minimum contour values are listed on the plots.

Fig 9. From top: the effect of velocity ratio on the tangential flow streamlines, pressure distribution, axial velocity profile and normalized apparent viscosity  $\mu/\mu_F$  for  $A=0.5$  and  $Re_U=1$ ,  $m=0.33$ . (a), (c), (e), (g)  $W/U=0.2$ , (b), (d), (f), (h)  $W/U=1$ . For streamlines and axial velocity the contour values at the surface are zero, only the maximum/minimum contour values are listed on the plots.

Fig 10. From top line : the effect of velocity ratio on the tangential flow streamlines, pressure distribution, axial velocity profile and normalized apparent viscosity  $\mu/\mu_F$  for  $A=0.5$  and  $Re_U=100$ ,  $m=0.33$ . (a), (c), (e), (g)  $W/U=0.01$ , (b), (d), (f), (h)  $W/U=0.2$ . For streamlines and axial velocity the contour values at the surface are zero, only the maximum/minimum contour values are listed on the plots.

Fig. A1. Frictional pressure gradient from lubrication equation A2 and duct flow equation A4. Solid lines: lubrication theory by Fitt and Please (2001); Dotted lines: duct flow results by Hartnett and Kostic (1989).

Table 1. Tabulated values of function  $f(m)$  in equation (A1) at various values of power law index  $m$ .

M	0.2	0.4	0.6	0.8	1.0
$f(m)$	0.0576	0.0977	0.1015	0.092868	0.08333

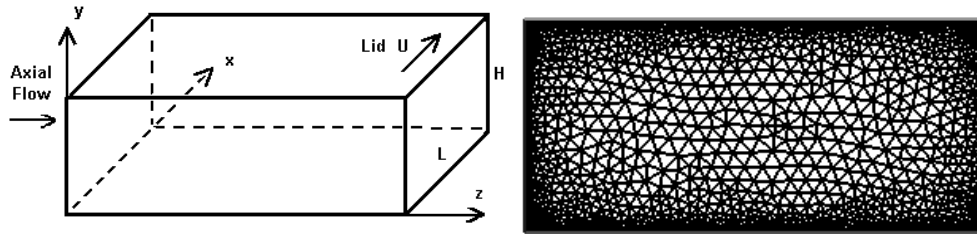


Fig. 1. (a) schematic view of the cavity, (b) mesh at aspect ratio  $A=0.5$  with 3470 elements.

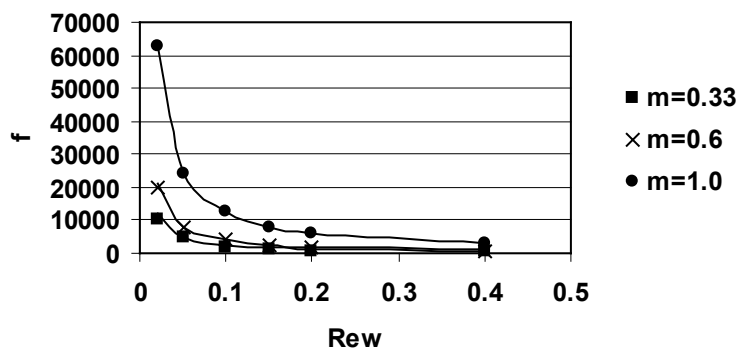
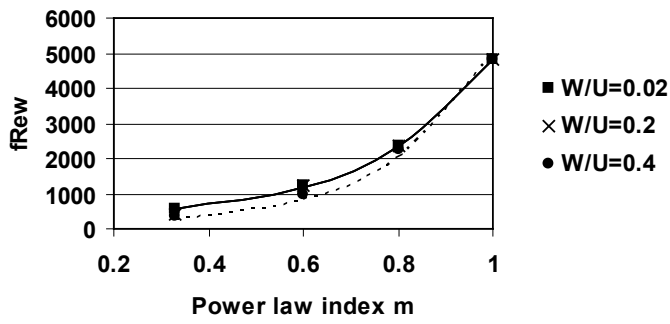
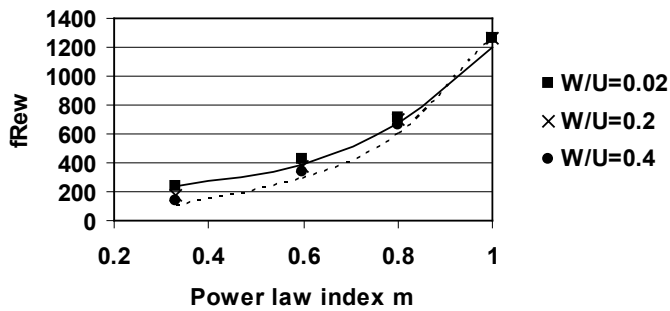


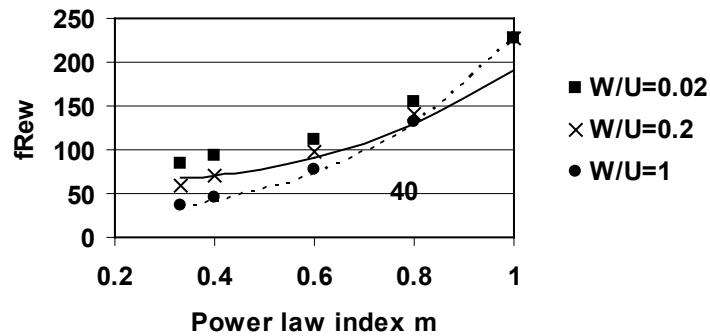
Fig. 2. Friction factor  $f$  as a function of  $Re_w$  for various value of power law index  $m$   $A=0.1$  and  $Re_U=1$ . Solid lines: lubrication theory; Symbols: computed values.



(a)



(b)



(c)

Fig. 3. Frictional pressure gradient at  $Re_U=1$ : (a)  $A=0.05$  and (b)  $A=0.1$  shows the effect of  $Re_W$  and  $m$ , (c)  $A=0.25$  the effect of velocity ratio. Solid lines: lubrication theory by Fitt and Please (2001); Dotted lines: duct flow results by Hartnett and Kostic (1989); Symbols: computed values.

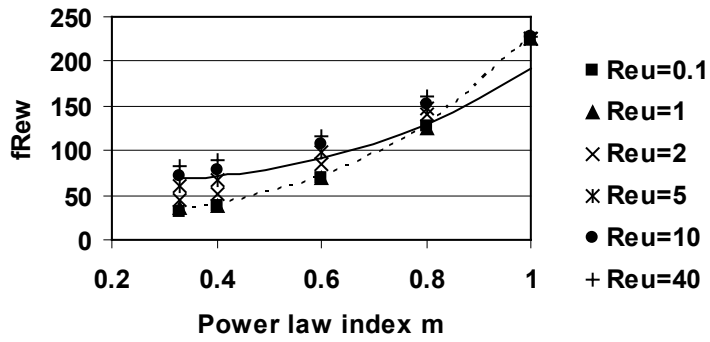


Fig. 4. Effect of tangential flow Reynolds number on  $f_{Rew}$  for  $A=0.25$  and  $Re_w=1$ . Solid lines: lubrication theory; Dotted lines: duct flow; Symbols: computed values.

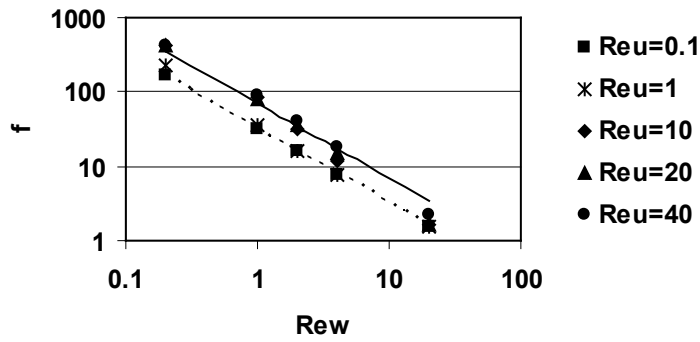
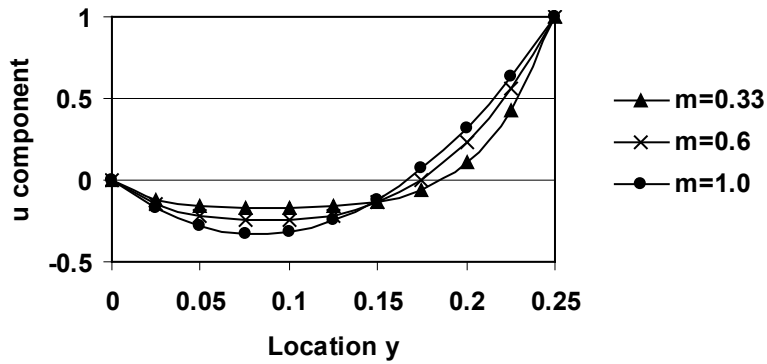
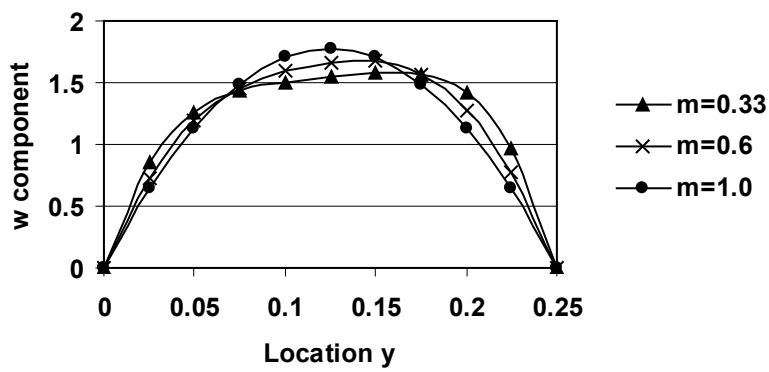


Fig. 5. Effect of tangential flow Reynolds number on  $f$  for  $A=0.25$ ,  $m=0.33$ . Solid lines: lubrication theory; Dotted lines: duct flow; Symbols: computed values.

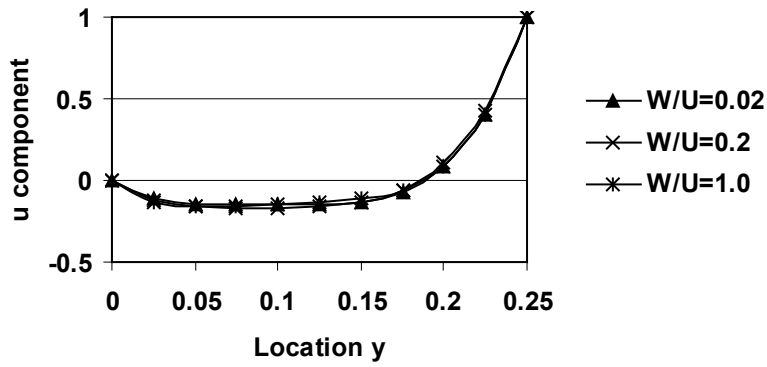


(a)

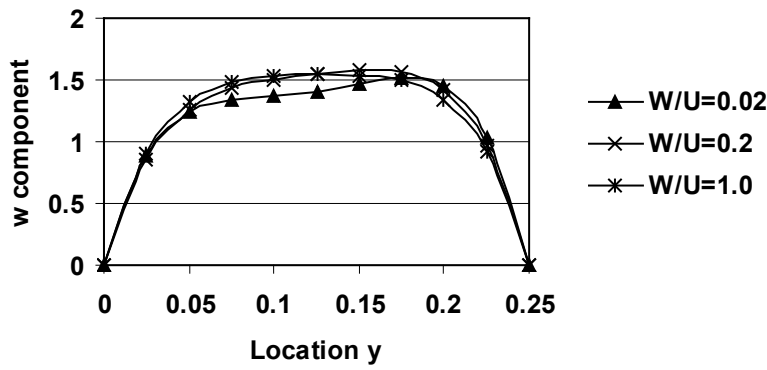


(b)

Fig. 6. Effect of shear thinning index  $m$  on the velocity profiles at the cavity centreline  $x=0.5$  for  $A=0.25$ ,  $Re_U=10$  and  $U/W=0.2$ . (a)  $u$  velocity component (b)  $w$  velocity component.



(a)



(b)

Fig. 7. Effect of velocity ratio on the velocity profiles at the cavity centreline  $x=0.5$  for  $A=0.25$ ,  $Re_U=10$ ,  $m=0.33$  and  $W/U=0.2$ . (a) u velocity component (b) w velocity component.

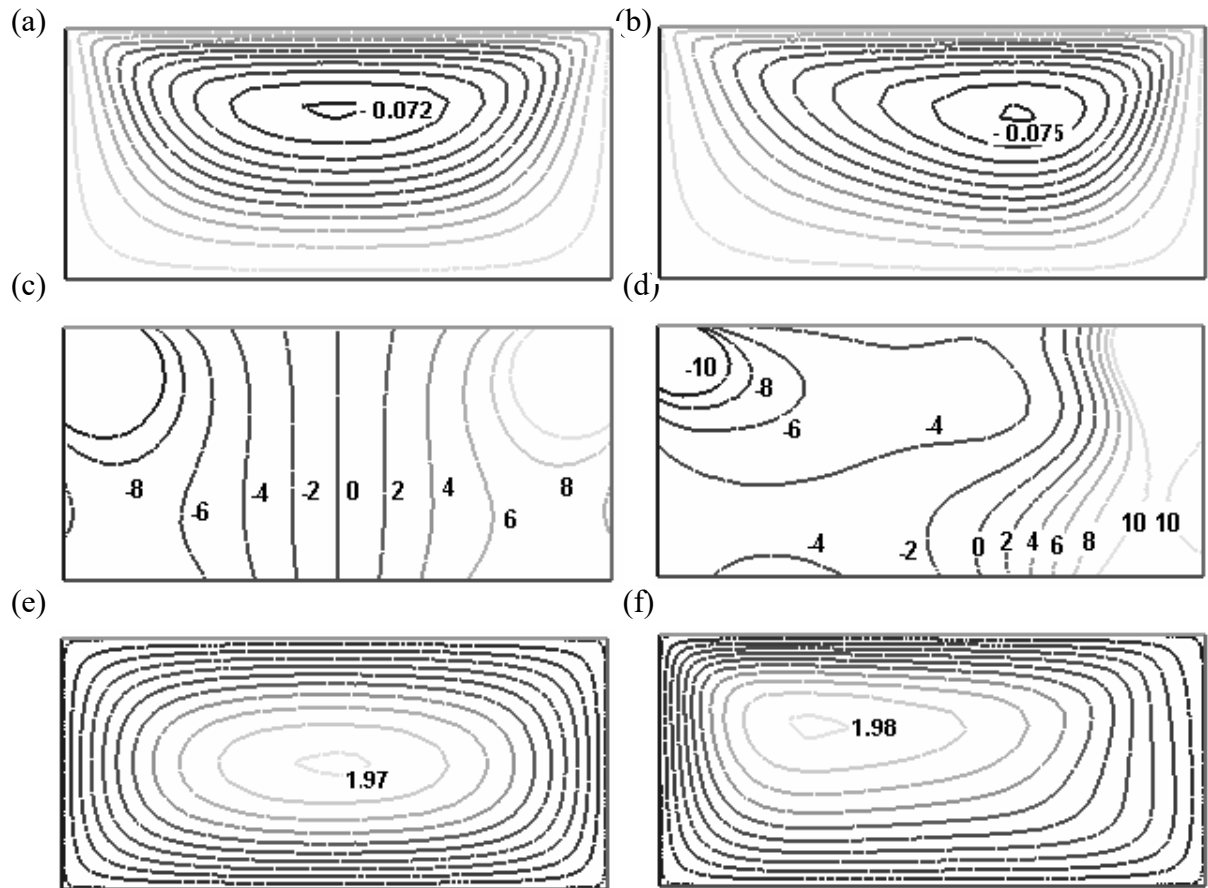


Fig 8. Effect of tangential flow Reynolds number on the tangential flow streamlines (top) pressure distribution (middle) and axial velocity profile (bottom) for  $A=0.5$  and  $Re_w=1$  with Newtonian fluid  $m=1$ . (a), (c), (e)  $Re_U=1$ , (b), (d), (f)  $Re_U=100$ . For streamlines and axial velocity the contour values at the surface are zero, only the maximum/minimum contour values are listed on the plots.

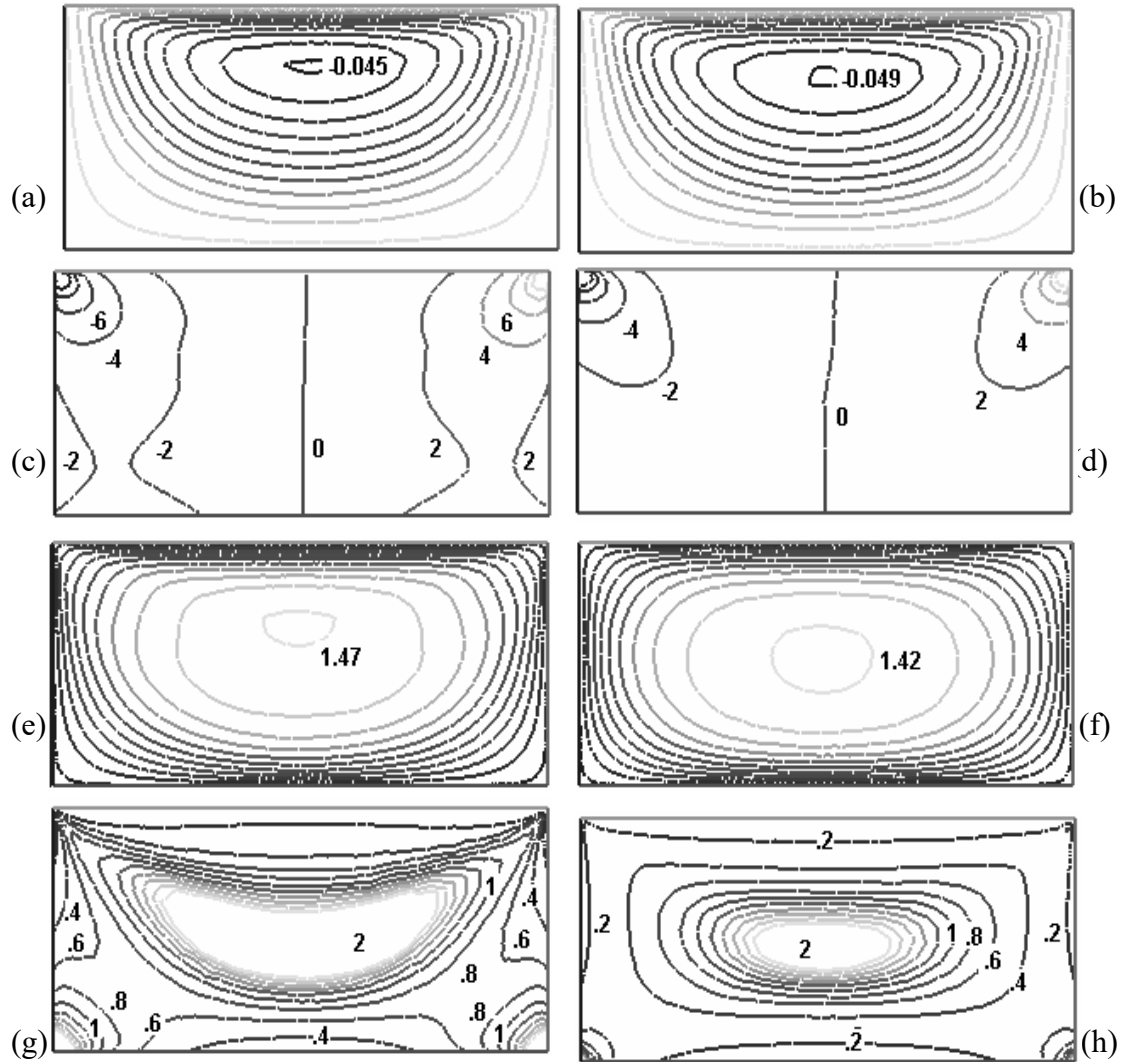


Fig 9. From top: the effect of velocity ratio on the tangential flow streamlines, pressure distribution, axial velocity profile and normalized apparent viscosity  $\mu/\mu_F$  for  $A=0.5$  and  $Re_U=1$ ,  $m=0.33$ . (a), (c), (e), (g)  $W/U=0.2$ , (b), (d), (f), (h)  $W/U=1$ . For streamlines and axial velocity the contour values at the surface are zero, only the maximum/minimum contour values are listed on the plots.

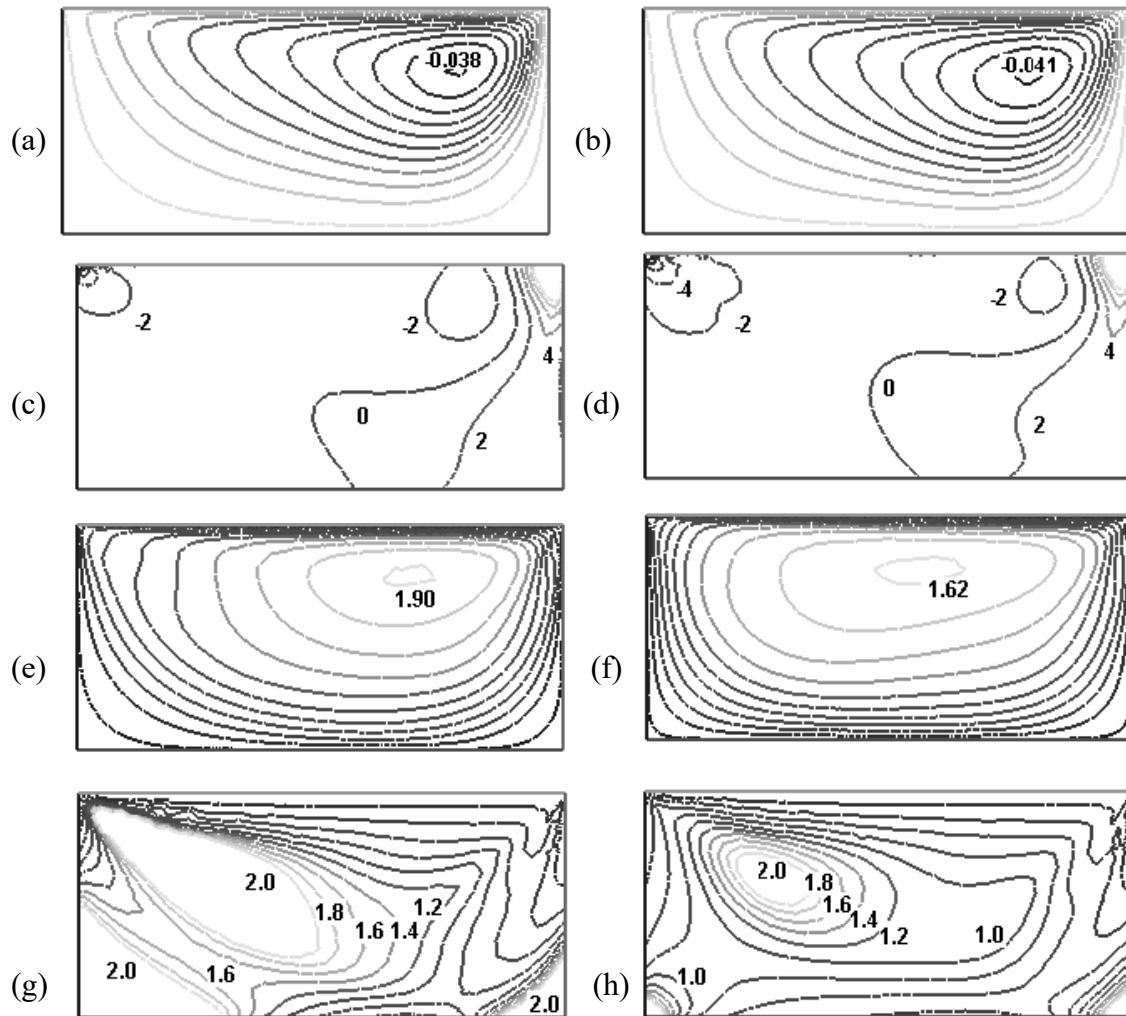


Fig 10. From top line : the effect of velocity ratio on the tangential flow streamlines, pressure distribution, axial velocity profile and normalized apparent viscosity  $\mu/\mu_F$  for  $A=0.5$  and  $Re_U=100$ ,  $m=0.33$ . (a), (c), (e), (g)  $W/U=0.01$ , (b), (d), (f), (h)  $W/U=0.2$ . For streamlines and axial velocity the contour values at the surface are zero, only the maximum/minimum contour values are listed on the plots.

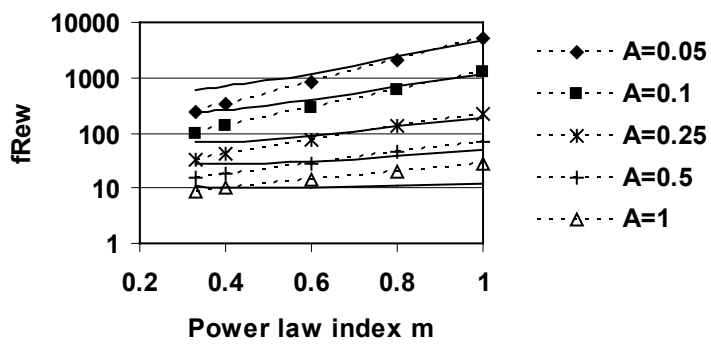


Fig. A1. Frictional pressure gradient from lubrication equation A2 and duct flow equation A4. Solid lines: lubrication theory by Fitt and Please (2001); Dotted lines: duct flow results by Hartnett and Kostic (1989).